Preferential CO oxidation in hydrogen-rich stream over Pt catalysts modified with alkali metals : Part II. Catalyst characterization and role of alkali metals

Hisanori Tanaka [a], Masatoshi Kuriyama [a], Yoichi Ishida [a], Shin-ichi Ito [a], Takeshi Kubota [b], Toshihiro Miyao [c], Shuichi Naito [c], Keiichi Tomishige [a,*], Kimio Kunimori [a,*]

[a] Institute of Materials Science, University of Tsukuba,1-1-1 Tennodai, Tsukuba, Ibaraki 305-8573, Japan
[b] Department of Material Science, Shimane University, Matsue 690-8504, Japan
[c] Department of Applied Chemistry, Faculty of Engineering, Kanagawa University, 3-27-1 Rokkakubashi, Kanagawa-ku, Yokohama, Kanagawa 221-8686, Japan

The promoting and negative effects of addition of alkali metals over Pt/Al_2O_3 in preferential CO oxidation in H_2-rich stream (PROX) were investigated in this work. The addition of alkali metals strongly influences the state of Pt metal particles, and coadsorbed species originating from H_2 and O_2 under the PROX condition can be found on highly active catalysts.

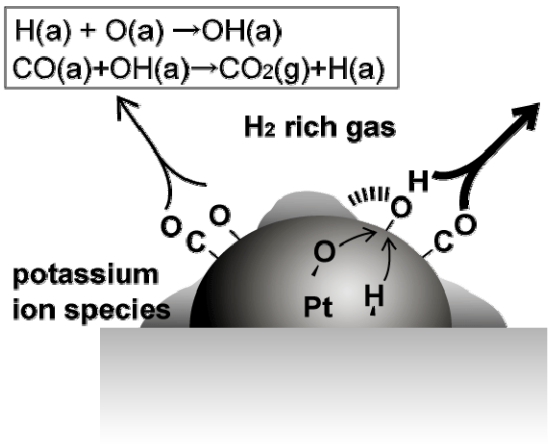

Preferential CO oxidation in hydrogen-rich stream over Pt catalysts modified with alkali metals : Part II. Catalyst characterization and role of alkali metals

Hisanori Tanaka [a], Masatoshi Kuriyama [a], Yoichi Ishida [a], Shin-ichi Ito [a], Takeshi Kubota [b], Toshihiro Miyao [c], Shuichi Naito [c], Keiichi Tomishige [a,*], Kimio Kunimori [a]

[a] Institute of Materials Science, University of Tsukuba,1-1-1 Tennodai, Tsukuba, Ibaraki 305-8573, Japan

[b] Department of Material Science, Shimane University, Matsue 690-8504, Japan

[c] Department of Applied Chemistry, Faculty of Engineering, Kanagawa University, 3-27-1 Rokkakubashi, Kanagawa-ku, Yokohama, Kanagawa 221-8686, Japan

Corresponding author

Keiichi Tomishige

Tel and Fax: +81-29-853-5030, E-mail: tomi@tulip.sannet.ne.jp

Abstract

The addition of alkali metals over Pt/Al_2O_3 has both promoting and negative effects on the

catalytic performance in the preferential CO oxidation in H_2-rich stream (PROX), therefore there is an optimum amount of alkali metal. The Pt/Al_2O_3 catalysts modified with Na, K, Rb and Cs were characterized by means of transmission electron microscopy (TEM), extended X-ray absorption fine structure (EXAFS), X-ray absorption near-edge structure (XANES), and Fourier transform infrared spectroscopy (FTIR). The results show that the addition of larger amount of alkali metals with stronger basicity causes the aggregation of Pt metal particles. The Pt particles on Pt/Al_2O_3 modified with alkali metals are more electron-deficient than those on Pt/Al_2O_3, and this weakens the strength of CO adsorption on Pt/Al_2O_3 modified with alkali metals, which is related to the enhancement of turnover frequency of the PROX. In addition, *in-situ* FTIR observation suggests that the coadsorbed species originating from H_2 and O_2 (e.g., the OH species) under the PROX condition, which promote the CO oxidation, can be found on highly active catalysts.

Keywords: preferential CO oxidation, platinum, alkali metals, potassium, OH group, FTIR, X-ray absorption fine structure

1. Introduction

Alkali metals are often used as additives to promote the catalytic activity and/or the selectivity of supported metal catalysts in some catalytic reactions. Recent studies indicate that introduction of alkali metals to supported metal catalysts is effective for the preferential oxidation of CO by O_2 in H_2-rich stream (PROX) [1-9]. Our group has reported that addition of potassium enhanced the catalytic performance of Rh/SiO_2 and Rh/USY [1, 2]. In both cases, there was an optimum additive

amount of potassium. The promoting effect of potassium is the enhancement of Rh dispersion on Rh/SiO_2, and it is the enhancement of turnover frequency of the PROX on Rh/USY. On both Rh catalysts, a negative effect of potassium can be due to covering of the surface of Rh metal particles with potassium species. In addition, the microstructure of $K\text{-}Rh/SiO_2$ was dependent on the method of catalyst preparation, and the relation between the catalytic performance in the PROX and the microstructure has been discussed [3].

Our group has also reported that Pt/Al_2O_3 modified with potassium is effective to the PROX, and the additive effect of potassium has been discussed [4-6]. Furthermore, the effect of alkali metals (Li, Na, K, Rb, Cs) on the PROX reaction over the Pt catalysts supported on Al_2O_3 has been investigated, and it is found that the catalytic performance is strongly affected by the basic strength and the additive amount of alkali metals [9]. In this work, the catalysts were characterized by transmission electron microscopy (TEM), extended X-ray absorption fine structure (EXAFS), X-ray absorption near-edge structure (XANES), and Fourier transform infrared spectroscopy (FTIR). The promoting and negative effects of the alkali metal addition on the catalytic performance are discussed on the basis of the catalyst characterization results.

2. Experimental

2.1. Catalyst preparation

The Pt/Al_2O_3 catalysts with and without the modification of potassium were prepared by the same method reported in our previous report [6]. The Pt/Al_2O_3 catalysts modified with sodium, rubidium and cesium were prepared in a similar way to Pt/Al_2O_3 modified with potassium, and a different

point is that precursors of sodium, rubidium and cesium were $NaNO_3$, $RbNO_3$ and $CsNO_3$, respectively. The loading amount of Pt was 2 wt%. The loading amount of alkali metals is described in the molar ratio to Pt (M/Pt), and the ratio was 3 and 10 in the present study. The modified Pt/Al_2O_3 catalysts are denoted as M-Pt/Al_2O_3, and M/Pt is shown in parenthesis like K-Pt/Al_2O_3 (10). All the M-Pt/Al_2O_3 catalysts were calcined at 773 K for 1 h. As a reference, Pt/Al_2O_3 catalysts calcined at higher temperatures (823, 873, 1073 K) were also prepared, and they were described with the calcination temperature in an angle bracket, for example, Pt/Al_2O_3 [773]. The catalysts were reduced with hydrogen at 773 K for 1 h as a pretreatment for the activity test and catalyst characterization.

2.2. Catalyst characterization

2.2.1. TEM observation

Transmission electron microscope (TEM) images were taken by means of JEM-2010F (JEOL) equipment operated at 200 kV. The catalysts were reduced by H_2 pretreatment at 773 K for 1 h in a fixed-bed reactor. Samples were dispersed in 2-propanol using supersonic waves, and they were put on Cu grids for TEM observation under air atmosphere. Average metal particle size (d) is calculated by $d = \Sigma n_i d_i^3 / \Sigma n_i d_i^2$ (n_i: number of pieces, d_i: particle size) [10].

2.2.2. EXAFS and XANES

Pt L_3-edge extended X-ray absorption fine structure (EXAFS) and X-ray absorption near edge structure (XANES) spectra were measured at the BL-12C station of the Photon Factory at the High Energy Accelerator Research Organization (Proposal No. 2005G041). The storage ring was operated at 2.5 GeV. A Si (111) single crystal was used to obtain a monochromatic X-ray beam. The

monochromator was detuned to 60% maximum intensity to avoid higher harmonics in the X-ray beam. Two ion chambers filled with Ar and 15 % Ar diluted N_2 for Pt L_3-edge EXAFS and XANES were used, respectively, as detectors of I and I_0. The samples for the measurement were prepared by pressing 200 mg of catalyst powder to disks. The thickness of the samples was chosen to be 0.6-0.7 mm (10 mmϕ) to give an edge jump of 0.7. The samples were pretreated with H_2 at 773 K for 1 h. After the pretreatment, we transferred the samples to the measurement cell without exposing the disk to air, using a glove box filled with nitrogen. EXAFS and XANES data were collected in a transmission mode at room temperature. For EXAFS analysis, the oscillation was first extracted from the EXAFS data by a spline smoothing method [11]. The oscillation was normalized by the edge height around 50 eV. The Fourier transformation of the k^3-weighted EXAFS oscillation from k space to r space was performed over the range 30-160 nm^{-1} to obtain a radial distribution function. The inversely Fourier filtered data were analyzed by a common curve-fitting method [12, 13]. For the curve-fitting analysis, the empirical phase shift and amplitude functions for Pt-Pt, Pt-O bonds were extracted from the data for Pt foil and $Na_2Pt(OH)_6$, respectively. Analysis of EXAFS data was performed using the "REX2000" program (Version: 2.3.3; Rigaku Corp.). In the analysis of XANES spectra, the normalized spectra were obtained by subtracting the pre-edge background from the raw data with a modified Victoreen's equation and normalizing them by the edge height [14-17].

2.2.3. FTIR measurements

FTIR spectra were recorded with a Nicolet Magna 550 spectrometer equipped with a MCT detector (resolution: 4 cm^{-1}) in a transmission mode, using an *in-situ* IR quartz cell with CaF_2

windows. All samples for the IR measurement were pressed into self-supporting wafers with a diameter of 20 mm and a weight of about 150 mg. The sample disk was transferred to the IR cell connected to the closed circulating vacuum systems for the observation of CO desorption profile when the sample temperature increases. The IR cell was connected to the flow systems for the observation during the preferential CO oxidation in hydrogen-rich stream. In the former case, the sample was reduced with H_2 at 773 K for 1 h in 30 ml·min^{-1} H_2 at the flow system as a pretreatment. In the experiments for the CO desorption profile, the sample after the pretreatment was cooled down to room temperature, and then it was exposed to 2.7 kPa CO for 15 min and evacuated. The spectra were obtained in the range of 313-433 K. In the experiments under the preferential CO oxidation reaction in hydrogen-rich stream, the sample was cooled down to 313 K after the pretreatment, and the reactant gases ($CO+O_2+H_2$) were introduced to the IR cell using the flow system. Temperature dependence of FTIR spectra during the reaction was measured for 15 min at each temperature. FTIR spectra of adsorbed species were obtained by subtracting the background spectra at the same temperature. The total flowing rate in the reactant gases was adjusted to GHSV=30,000 h^{-1}, which was used for the activity tests in the fixed bed reactor.

3. Results and discussion

3.1. TEM observation

Figure 1 shows TEM images of Pt/Al_2O_3 [773], K-Pt/Al_2O_3 (3 and 10) and Cs-Pt/Al_2O_3 (3 and 10). The average particle sizes of Pt/Al_2O_3 [773] and K-Pt/Al_2O_3 (3) were smaller than those of other three catalysts, and they were determined to be 0.5±0.1 nm and 0.6±0.1 nm, respectively, which

are supported by high dispersion on the basis of CO adsorption (CO/Pt=0.52, 0.46). Average particle size of K-Pt/Al_2O_3 (10) was determined to be 2.0±0.3 nm. Those of Cs-Pt/Al_2O_3 (3 and 10) were estimated to be 1.7±0.2 nm and 3.8±0.3 nm, respectively. From the comparison, it is found that the modification by larger amount of alkali metals with stronger basicity increased the average particle size of Pt.

3.2. EXAFS and XANES

Figure 2 shows the result of Pt L_3-edge EXAFS analysis of the catalysts. Curve fitting results are listed in Table 1. The Pt-Pt and Pt-O bonds were required for the curve fitting of Pt/Al_2O_3 [773] and [823], although the contribution of the Pt-O bond was rather small. This suggests that highly dispersed Pt metal particles interact with the surface of the Al_2O_3 support. The coordination numbers of the Pt-Pt bond on Pt/Al_2O_3 increased monotonously with increasing calcination temperature. This behavior corresponds to the aggregation by the calcination at higher temperature. In the case of the M-Pt/Al_2O_3 (3) (M = Na, K, Rb, Cs), the Pt-Pt and Pt-O bonds were necessary. The coordination number of the Pt-Pt bond on M-Pt/Al_2O_3 (3) was a little larger than that on Pt/Al_2O_3 [773], which is consistent with the TEM results. On the other hand, the spectra of M-Pt/Al_2O_3 (10) were fitted by only the Pt-Pt bond, and the coordination number increased more remarkably by the addition of alkali metals with stronger basicity.

Figure 3 shows Pt L_3-edge XANES spectra of the catalysts, and Table 2 gives the results of XANES analysis. The white line intensity of Pt L_3-edge is known to be an informative indication of the electron state of Pt; the larger white line is due to the greater electron vacancy in d-orbital [18]. As reported previously, a relative electron deficiency of the Pt species can be determined based on

the white line intensity [14-17]. For the Pt/Al_2O_3 catalysts, the relative electron deficiency decreased gradually with increasing calcination temperature. This tendency is related to the increase of the coordination number of the Pt-Pt bond and the decrease of that of the Pt-O bond in the EXAFS results, which means the aggregation by the calcination at higher temperature. The electron deficiency of M-Pt/Al_2O_3 (3) was much more significant than that of Pt/Al_2O_3 [773]. The difference in the electron deficiency was small among the M-Pt/Al_2O_3 (3) catalysts. On the other hand, the electron deficiency of M-Pt/Al_2O_3 (10) was strongly dependent on the kind of alkali metals, and the order was Na > K > Rb > Cs. As described above, the electron deficiency can be influenced by the particle size of Pt and the kind of alkali metals.

To facilitate discussion on the electron state of the catalysts considering the Pt metal particle size, the relationship between the coordination number of the Pt-Pt bond obtained from EXAFS and the relative electron deficiency from XANES is plotted in Figure 4. In the case of the Pt/Al_2O_3 catalysts, the relative electron deficiency decreased gradually with increasing coordination number (CN) of the Pt-Pt bond. Smaller particles have more interaction with the oxide ions on the Al_2O_3 surface. This can explain the relation between the electron deficiency and the CN of the Pt-Pt bond. On the other hand, the points due to M-Pt/Al_2O_3 (3) catalysts are located in the range of 0.16~0.19 relative electron deficiency and 7~8 CN of the Pt-Pt bond. From the comparison between M-Pt/Al_2O_3 (3) and Pt/Al_2O_3 [823], which gave similar CN of Pt-Pt bond, the Pt particles on M-Pt/Al_2O_3 (3) is much more electronically deficient than those on Pt/Al_2O_3 [823]. This means the electron transfer from the Pt particles to the alkali metal species. This phenomenon is opposite to the case of the interaction between metal surfaces and metallic alkali metal species [19-21]. Electron transfer from

metallic alkali metal species to metal surfaces is explained by the scheme of $M^0 \rightarrow M^+ + e^-$ (M = alkali metals) [19-21]. In the present case, the alkali metals are added as an ionic species, and the electron transfer from the Pt metal to the alkali metals can be explained by the interaction between the electrons in the Pt metal and alkali metal ions. Similar tendency has been reported in the case of the modification of alkali metal ions [22, 23].

On the other hand, in the case of M-Pt/Al_2O_3 (10), the degree of the electron transfer became smaller. The EXAFS analysis showed that larger additive amount of alkali metal ions caused the aggregation of metal particles, which can be due to the neutralization of the surface acidity of Al_2O_3 [24, 25]. When the particle size increases, the ratio of the surface Pt atoms to the total atoms became smaller. Since the Pt metal particles interact with alkali metal ions through the surface Pt atom, the decrease of the electron deficiency can be related to the decrease the number of surface Pt atoms. The alkali metal ions with stronger basicity promoted the aggregation of Pt particles and decreased the electron deficiency. The electronic state of the Pt metal particles can affect the strength of the CO adsorption [26, 27]. According to the previous reports, the weakening of the CO adsorption can promote the PROX activity [6, 8, 28, 29]. Therefore, the desorption profiles of adsorbed CO were measured by FTIR.

3.3. Desorption profile of adsorbed CO by FTIR

Figures 5 and 6 show the effect of the evacuation temperature on IR spectra of adsorbed CO on the catalysts. On Pt/Al_2O_3 [773], a sharp peak due to linear CO at 2061 cm^{-1} was mainly observed. In the case of M-Pt/Al_2O_3 (3), the main peak was also assigned to linear CO, although the peak

became broader and the wavenumber shift of linear CO is not so significant. In contrast, the intensity of a smaller peak with lower wavenumber (1750~1850 cm^{-1}) appears to be higher. On the other hand, the spectra of CO adsorption on M-Pt/Al_2O_3 (10) were different from those on Pt/Al_2O_3 and M-Pt/Al_2O_3 (3) in Figure 6. On M-Pt/Al_2O_3 (10), three peaks were observed. The peaks at 2059-2049 cm^{-1} and 1970-1979 cm^{-1} can be assigned to linear and bridge CO on Pt, respectively [6, 30, 31]. It should be noted that the peak at 1748-1785 cm^{-1} was very weak on Pt/Al_2O_3: it has been suggested that this peak can be assigned to a threefold-coordinated CO species on the Pt atoms interacting with alkali metal species [6, 30, 31]. The peak position of linear CO on M-Pt/Al_2O_3 (10) was not so different from that on M-Pt/Al_2O_3 (3) and Pt/Al_2O_3. From the comparison, it is found that the larger amount of alkali metal addition influenced the surface state of Pt metal particles strongly. From the results of the XANES analysis, it doesn't seem that this effect is due to the electronic modification of Pt metal particles with alkali metal species. In fact, the XANES analysis reflects the total property including the surface and bulk of metal particles. In contrast, the FTIR of CO adsorption can focus on the surface state of Pt metal particles modified with alkali metal species. As a result of the XANES analysis and FTIR observation, the added alkali metals changed and modified the surface state of Pt metal particles drastically, and this suggests the presence of alkali metal species loaded on the surface of Pt metal particles.

Furthermore, attentions should be paid on the desorption profile of adsorbed CO. Figure 7 shows the total area of the CO adsorption peaks as a function of evacuation temperature on the basis of Figures 5 and 6. The profiles indicate that CO adsorbed on M-Pt/Al_2O_3 (3 and 10) catalysts was desorbed at temperatures lower than that on Pt/Al_2O_3. However, the difference among the

M-Pt/Al_2O_3 catalysts is rather small. In the case of M-Pt/Al_2O_3 (3), it can be interpreted that the electron deficient Pt surface, which is indicated by the XANES analysis, weaken the interaction between CO and Pt, although the shift of the peak position of linear CO to higher wavenumber was not observed clearly. On the other hand, in the case of M-Pt/Al_2O_3 (10), it is thought that the change of the CO adsorption site from linear to bridge and threefold can be related to the weakening the interaction between CO and Pt. This behavior can explain why the addition of alkali metals enhanced the activity of the CO+O_2 reaction in the absence of H_2 [9]. It has been known that the reaction order with respect to CO in the CO+O_2 reaction is negative because the adsorption of CO is strong at lower reaction temperature [32]. Therefore, when the CO adsorption becomes weaker, the CO coverage can be decreased and the oxygen coverage can be increased, and this can promote the CO+O_2 reaction. In addition, the result also agrees well that all these M-Pt/Al_2O_3 (3 and 10) catalysts gave higher turnover frequency (TOF) in the preferential CO oxidation in H_2-rich stream than the Pt/Al_2O_3. However, the result cannot explain very high TOF of K-Pt/Al_2O_3 (10) and Cs-Pt/Al_2O_3 (3) [9].

Figure 8 shows the results of *in-situ* FTIR measurement of the catalysts during the PROX reaction. On Pt/Al_2O_3, when the reaction temperature increased from 313 to 393 K, the change of the FTIR peaks in terms of the position and the area was so small (Fig. 8 (a)), and in the case of Cs-Pt/Al_2O_3 (10), the change was also small (Fig. 8 (d)). In contrast, the peak positions of linear, bridge and threefold CO were shifted from 2073, 2010, 1802 to 2060, 1970, 1776 cm^{-1}, respectively, when the catalysts were heated from 313 to 393 K on K-Pt/Al_2O_3 (10) (Fig. 8 (b)). At the same time, the total area of the three peaks decreased to 63 %. On Cs-Pt/Al_2O_3 (3), the positions of the three

peaks also moved to lower wavenumber remarkably, and the total area decreased to 83 % (Fig. 8 (c)). Since the temperature dependence of the FTIR peaks is strong on the catalysts with higher TOF and it is weak on the catalysts with lower TOF, it seems that the profile of the temperature dependence is associated with the catalytic performance. As reported previously [6], when only CO is present in the gas phase, the coverage of CO is close to the saturation level at the reaction temperature range. Therefore, the decrease of the total area with increasing the reaction temperature is connected to the coverage increase of coadsorbed species, and this can promote the CO oxidation. One possible candidate is the OH group, which can be formed by adsorbed hydrogen and oxygen atoms [33-36]. This is also supported by the previous reports on the promotion of the CO oxidation by the OH group on Pt (111) [37, 38].

$$H\,(a) + O\,(a) \rightarrow OH\,(a)$$

$$CO\,(a) + OH\,(a) \rightarrow CO_2\,(g) + H\,(a)\ [(a) : \text{adsorbed, } (g) : \text{gas phase}]$$

These reaction formulas correspond to the reaction route via OH species as an autocatalytic mechanism. In fact, the presence of H_2 enhances the CO oxidation activity on K-Pt/Al_2O_3 (10) [5, 6]. At present, we did not succeed in direct observation of the OH group by *in-situ* FT-IR because of the interference of H_2O as a byproduct in the PROX. Judging from the decrease of the peak area during the increase of temperature, the coverage of coadsorbed species is higher on K-Pt/Al_2O_3 (10) and Cs-Pt/Al_2O_3 (3) than that on Pt/Al_2O_3 and Cs-Pt/Al_2O_3 (10), and the coverage is related to the catalytic activity. Alkali metals can contribute to the enhancement of the coverage of the coadsorbed species, for example, by Coulomb interaction between OH^- and alkali ion species. In addition, considering that the activity of the water gas shift reaction is very low [6, 9], this active OH cannot

be formed from H_2O in the gas phase. Promoting effect of potassium was most remarkable in the PROX. This suggests that the medium basicity of potassium can cause suitable strength of the interaction between the OH group and the alkali metal ion species. On the catalyst with large additive amount of strong basic alkali metal like Cs-Pt/Al_2O_3 (10), the activity of the PROX was very low. This can be because too strong interaction between the OH group and the alkali metal ion species decrease the reactivity of the OH group.

4. Conclusions

1) Metal particle size of Pt on Pt/Al_2O_3 with modification of alkali metals is strongly influenced by the kind and the amount of added alkali metals. Addition of alkali metals with stronger basicity causes the aggregation of Pt metal particles, and addition of larger amount of alkali metals also causes the aggregation from the results of TEM observation and EXAFS analysis.

2) From the combination of XANES with EXAFS analysis, Pt particles on Pt/Al_2O_3 modified with alkali metals were more electron-deficient than those on Pt/Al_2O_3 with similar Pt particle size without the modification.

3) The strength of CO adsorption on Pt/Al_2O_3 is weakened by the addition of alkali metals, however, the additive effect is not so dependent on the kind and amount of alkali metals.

4) The adsorbed CO species on M-Pt/Al_2O_3 (3) were similar to those on Pt/Al_2O_3 from the result of FTIR obsearvation. However, those on M-Pt/Al_2O_3 (10) were different. The addition of large amount of alkali metals gave the bridge and threefold CO, which suggests that the surface of Pt particles was modified directly with alkali metal species.

5) *In-situ* FT-IR observation under the PROX condition on K-Pt/Al_2O_3 (10) and Cs-Pt/Al_2O_3 (3), which gave much higher TOF in the PROX than Pt/Al_2O_3 and Cs-Pt/Al_2O_3 (10), suggests that the coadsorbed species originating from H_2 and O_2 (e.g., the OH species), which promote the CO oxidation, can be present on the Pt surface.

References

[1] H. Tanaka, S. Ito, S. Kameoka, K. Tomishige, K. Kunimori, Catal. Commun. 4 (2003) 1.

[2] H. Tanaka, S. Ito, S. Kameoka, K. Tomishige, K. Kunimori, Appl. Catal. A: Gen. 250 (2003) 255.

[3] S. Ito, H. Tanaka, Y. Minemura, S. Kameoka, K. Tomishige, K. Kunimori, Appl. Catal. A: Gen. 273 (2004) 295.

[4] Y. Minemura, S. Ito, T. Miyao, S. Naito, K. Tomishige, K. Kunimori, Chem. Commun. (2005) 1429.

[5] Y. Minemura, M. Kuriyama, S. Ito, K. Tomishige, K. Kunimori, Catal. Commun. 7 (2006) 623.

[6] M. Kuriyama, H. Tanaka, S. Ito, T. Kubota, T. Miyao, S. Naito, K. Tomishige, K. Kunimori, J. Catal. 252 (2007) 39.

[7] C. Pedrero, T. Waku, E. Iglesia, J. Catal. 233 (2005) 242.

[8] N. Iwasa, S. Arai, M. Arai, Appl. Catal. B: Environ. 79 (2007) 132.

[9] H. Tanaka, M. Kuriyama, Y. Ishida, S. Ito, K. Tomishige, K. Kunimori, Appl. Catal. A: Gen., submitted.

[10] Y. Chen, K. Tomishige, K. Yokoyama and K. Fujimoto, Appl. Catal. A: Gen. 165 (1997) 335.

[11] J. W. Cook, D. E. Sayers, J. Appl. Phys. 52 (1981) 5024.

[12] K. Okumura, J. Amano, N. Yasunobu and M. Niwa, J. Phys. Chem. B 104 (2000) 1050.

[13] K. Okumura, S. Matsumoto, N. Nishiaki and M. Niwa, Appl. Catal. B: Environ. 40 (2003) 151.

[14] T. Kubota, K. Asakura, N. Ichikuni, Y. Iwasawa, Chem. Phys. Lett., 256 (1996) 445.

[15] T. Kubota, K. Asakura, Y. Iwasawa, Catal. Lett. 46 (1997) 141.

[16] A. N. Mansour, J. W. Cook, Jr., D. E. Sayers, J. Phys. Chem. 88 (1984) 2330.

[17] J. A. Horsely, J. Chem. Phys. 76 (1982) 1451.

[18] H. Yoshida, Y. Yazawa, T. Hattori, Catal. Today 87 (2003) 19.

[19] H. P. Bonzel, Surf. Sci. Rep. 8 (1987) 43.

[20] Y. Matsumoto, K. Watanabe, N. Takagi, Surf. Sci. 593 (2005) 110.

[21] S. J. Pratt, D. A. King, Surf. Sci. 540 (2003) 185.

[22] L. F. Liotta, G. A. Martin, G. Deganello, J. Catal. 164 (1996) 322.

[23] A. Lucas-Consuegra, F. Donando, J. L. Valverde, R. Karoum, P. Vernoux, Catal. Commun. 9 (2008) 17.

[24] C. Bisio, K. Fajerwerg, G. Marta, P. Massiani, Catal. Today 124 (2007) 36.

[25] F. J. Maladonado, T. Bécue, J. M. Silva, M. F. Ribeiro, P. Massiani, M. Kermarec, J. Catal. 195 (2000) 342.

[26] O. Lorret, S. Morandi, F. Prinetto, G. Ghiotti, D. Tichit, R. Durand, B. Coq, Micopor. Mesopor. Mater. 103 (2007) 48.

[27] T. Okuhara, H. Tamura, M. Misono, J. Catal. 95 (1985) 41.

[28] S. Guerrero, J. T. Miller, E. E. Wolf, Appl. Catal. A: Gen. 328 (2007) 27.

[29] S. H. Cho, J. S. Park, S. H. Choi, S. K. Lee, S. H. Kim, Catal. Lett. 103 (2005) 257.

[30] S. Derrouiche, P. Gravejat, B. Bassou, D. Bianchi, Appl. Surf. Sci. 253 (2007) 5894.

[31] J. Bodis, C. Nemeth, J. Mink, G. Keresztury, P. Tetenyi, J. Mol. Struct. 410-411 (1997) 179.

[32] K. Nakao, S. Ito, K. Tomishige, K. Kunimori, J. Phys. Chem. B 109 (2005) 24002.

[33] A. Fukuoka, J. Kimura, T. Oshio, Y. Sakamoto, M. Ichikawa, J. Am. Chem. Soc. 129 (2007)

10120.

[34] A. Manasilp, E. Gulari, Appl. Catal. B: Environ. 37 (2002) 17.

[35] A. B. Mhadeshwar, D. G. Vlachos, J. Phys. Chem. B 108 (2004) 15246.

[36] Y. Sato, M. Koizumi, T. Miyao, S. Naito, Catal. Today 111 (2006) 164.

[37] I. N. Yakovkin, V. I. Chernyi, A. G. Naumovets, Surf. Sci. 442 (1999) 81.

[38] J. Bergeld, B. Kasemo, D. V. Chakarov, Surf. Sci. 495 (2001) L815.

Table 1 Curve fitting results of Pt-L_3 edge EXAFS of Pt/Al_2O_3 and M-Pt/Al_2O_3 (M = Na, K, Rb, Cs) catalysts.

Catalysts	Shells	CN [a]	R / 10^{-1} nm [b]	σ / 10^{-1} nm [c]	ΔE_0 / eV [d]	R_f / % [e]
Pt/Al_2O_3 [773]	Pt-Pt	5.9±0.7	2.65±0.007	0.094±0.007	-4.7±1.8	0.9
	Pt-O	0.9±0.2	2.03±0.026	0.065±0.044	-5.7±7.1	
Pt/Al_2O_3 [823]	Pt-Pt	7.6±0.6	2.78±0.002	0.093±0.002	6.5±0.5	1.0
	Pt-O	0.6±0.5	2.12±0.030	0.092±0.066	2.0±6.9	
Pt/Al_2O_3 [873]	Pt-Pt	9.5±0.4	2.78±0.002	0.082±0.001	1.6±0.6	0.7
Pt/Al_2O_3 [1073]	Pt-Pt	11.1±0.2	2.77±0.002	0.072±0.003	1.8±0.6	1.0
Na-Pt/Al_2O_3 (3)	Pt-Pt	7.5±0.5	2.70±0.012	0.105±0.04	0.9±2.5	1.4
	Pt-O	2.5±0.3	2.03±0.020	0.088±0.026	-2.0±4.5	
Na-Pt/Al_2O_3 (10)	Pt-Pt	8.3±0.6	2.75±0.003	0.081±0.004	1.2±0.8	0.9
K-Pt/Al_2O_3 (3)	Pt-Pt	7.5±0.5	2.71±0.013	0.105±0.004	-0.7±2.7	1.2
	Pt-O	2.5±0.7	2.04±0.021	0.089±0.027	-3.4±4.7	
K-Pt/Al_2O_3 (10)	Pt-Pt	8.5±0.3	2.74±0.003	0.080±0.012	-0.2±0.8	0.7
Rb-Pt/Al_2O_3 (3)	Pt-Pt	7.4±0.5	2.71±0.011	0.101±0.011	-0.6±2.5	1.3
	Pt-O	2.8±0.3	2.04±0.022	0.094±0.028	-1.2±4.7	
Rb-Pt/Al_2O_3 (10)	Pt-Pt	9.2±0.5	2.75±0.002	0.075±0.003	0.7±0.7	0.9
Cs-Pt/Al_2O_3 (3)	Pt-Pt	7.9±0.3	2.74±0.005	0.090±0.007	3.4±1.4	1.3
	Pt-O	1.8±0.3	2.08±0.024	0.081±0.032	-0.9±5.6	
Cs-Pt/Al_2O_3 (10)	Pt-Pt	10.2±0.2	2.75±0.002	0.072±0.002	0.6±0.5	0.5

Sample pretreatment: reduction (H_2, 773 K, 1 h).

[a] Coordination number. [b] Bond distance. [c] Debye-Waller factor. [d] Difference in the origin of photoelectron energy between the reference and the sample. [e] Residual factor. Fourier filtering range: 0.14-0.31 nm

Table 2 Result of Pt-L_3 edge XANES analysis of of Pt/Al_2O_3 and M-Pt/Al_2O_3 (M = Na, K, Rb, Cs) catalysts.

Catalyst	ΔA [a]	A [b]	$\Delta A / A$ [c]
Pt/Al_2O_3 [773]	0.83	-	0.108
Pt/Al_2O_3 [823]	0.66	-	0.085
Pt/Al_2O_3 [873]	0.58	-	0.074
Pt/Al_2O_3 [1073]	0.49	-	0.062
Na-Pt/Al_2O_3 (3)	1.34	-	0.174
Na-Pt/Al_2O_3 (10)	0.99	-	0.128
K-Pt/Al_2O_3 (3)	1.44	-	0.187
K-Pt/Al_2O_3 (10)	0.78	-	0.102
Rb-Pt/Al_2O_3 (3)	1.37	-	0.178
Rb-Pt/Al_2O_3 (10)	0.78	-	0.101
Cs-Pt/Al_2O_3 (3)	1.27	-	0.166
Cs-Pt/Al_2O_3 (10)	0.65	-	0.085
Pt foil	0.0	7.70	0

[a] Area difference between catalysts and Pt-foil (11540-11575 eV).

[b] White line area of Pt foil.

[c] Relative electron deficiency.

Figure Captions

Fig. 1 TEM images of the catalysts after H_2 reduction.

Fig. 2 Results of Fourier transform of k^3-weighted Pt L_3-edge EXAFS oscillations (Ⅰ～Ⅲ) and the curve fitting (Ⅳ) of the catalysts after the H_2 reduction.
(Ⅰ) Pt/Al_2O_3 calcined at various temperatures, (Ⅱ) M-Pt/Al_2O_3 (3) (M = Na, K, Rb, Cs), (Ⅲ) M-Pt/Al_2O_3 (10) (M = Na, K, Rb, Cs). (Ⅳ) solid line (observed) and broken line (calculated). FT range: 30-160 nm^{-1} (Pt/Al_2O_3, M-Pt/Al_2O_3 (10)) or 30-135 nm^{-1} (M-Pt/Al_2O_3 (3)).

Fig. 3 Pt L_3-edge XANES spectra of the catalysts after H_2 reduction.
(Ⅰ) Pt/Al_2O_3 calcined at various temperatures,
(Ⅱ) M-Pt/Al_2O_3 (3) (M = Na, K, Rb, Cs),
(Ⅲ) M-Pt/Al_2O_3 (10) (M = Na, K, Rb, Cs).

Fig. 4 Relation between the relative electron deficiency from XANES and the coordination number (CN) of the Pt-Pt bond from EXAFS.
(◆) Pt/Al_2O_3 calcined at various temperatures,
(◇) M-Pt/Al_2O_3 (3 and 10) (M = Na, Ka, Rb, Cs).

Fig. 5 Effect of evacuation temperature on IR spectra of adsorbed CO on Pt/Al_2O_3 [773] and M-Pt/Al_2O_3 (3) catalysts. The samples were exposed to 0.3 kPa CO at 313 K and evacuated.

Fig. 6 Effect of evacuation temperature on IR spectra of adsorbed CO on M-Pt/Al_2O_3 (10) catalysts. The samples were exposed to 0.3 kPa CO at 313 K and evacuated.

Fig. 7 Effect of evacuation temperature on the decrease in the total area of the CO peaks (Figs. 5 and 6). Pt/Al_2O_3 (×), Na-Pt/Al_2O_3 (3 (●) and 10 (○)), K-Pt/Al_2O_3 (3 (◆) and 10 (◇)), Cs-Pt/Al_2O_3 (3 (▲) and 10 (△)). The samples were exposed to 0.3 kPa CO at 313 K and evacuated.

Fig. 8 Effect of reaction temperature on IR spectra of the catalysts under the PROX condition (0.2% CO, 0.2% O_2, 75 % H_2, He balance).
——: 313 K, ——: 353 K, ——: 393 K, ——: 433 K.

a) Pt/Al_2O_3 [773]

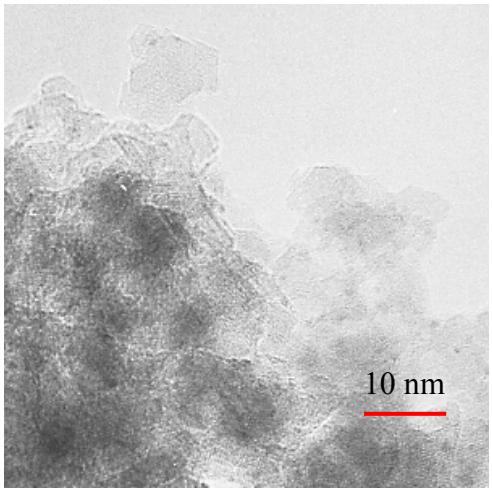

b) K- Pt/Al_2O_3 (3)

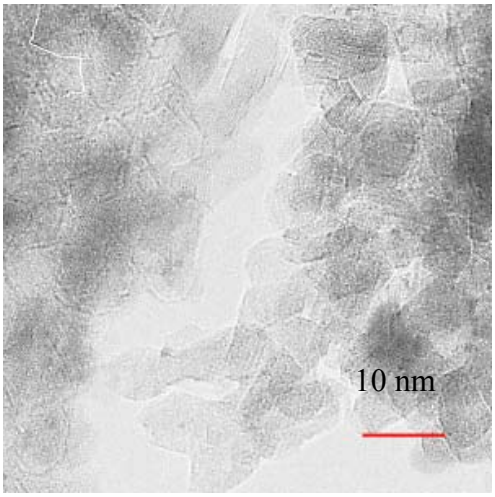

d) Cs- Pt/Al_2O_3 (3)

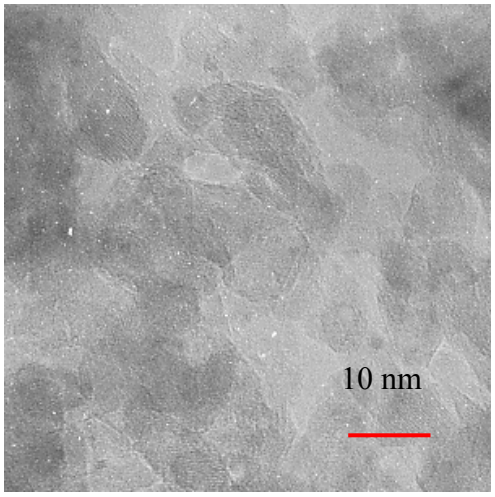

c) K- Pt/Al_2O_3 (10)

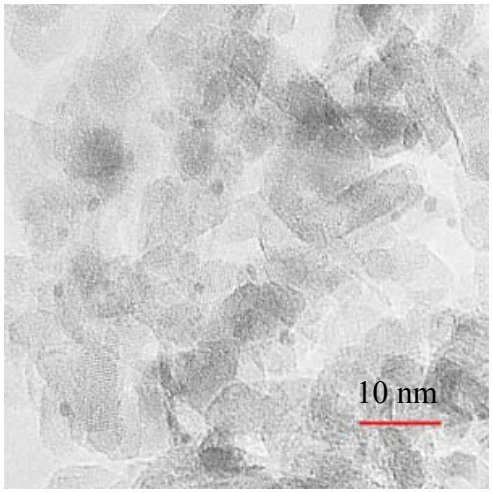

d) Cs- Pt/Al_2O_3 (10)

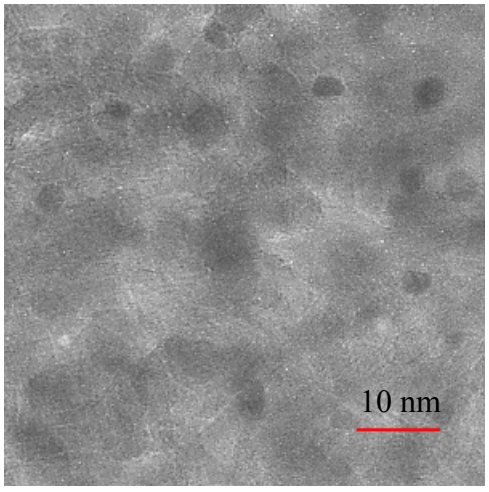

Fig. 1 TEM images of the catalysts after H_2 reduction.

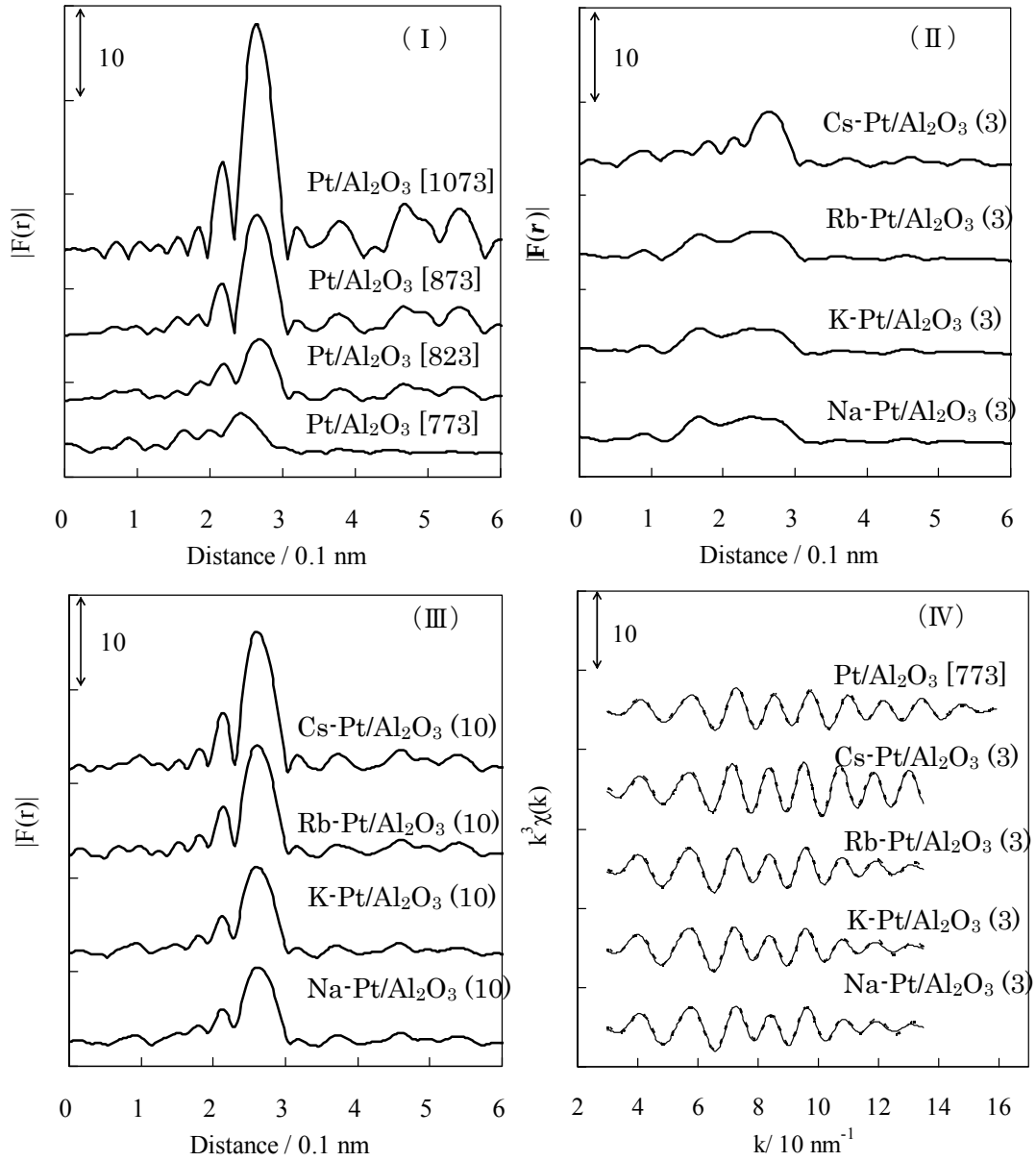

Fig. 2 Results of Fourier transform of k^3-weighted Pt L_3-edge EXAFS oscillations (Ⅰ～Ⅲ) and the curve fitting (Ⅳ) of the catalysts after the H_2 reduction.
(Ⅰ) Pt/Al_2O_3 calcined at various temperatures, (Ⅱ) M-Pt/Al_2O_3 (3) (M = Na, K, Rb, Cs), (Ⅲ) M-Pt/Al_2O_3 (10) (M = Na, K, Rb, Cs). (Ⅳ) solid line (observed) and broken line (calculated).
FT range: 30-160 nm^{-1} (Pt/Al_2O_3, M-Pt/Al_2O_3 (10)) or 30-135 nm^{-1} (M-Pt/Al_2O_3 (3)).

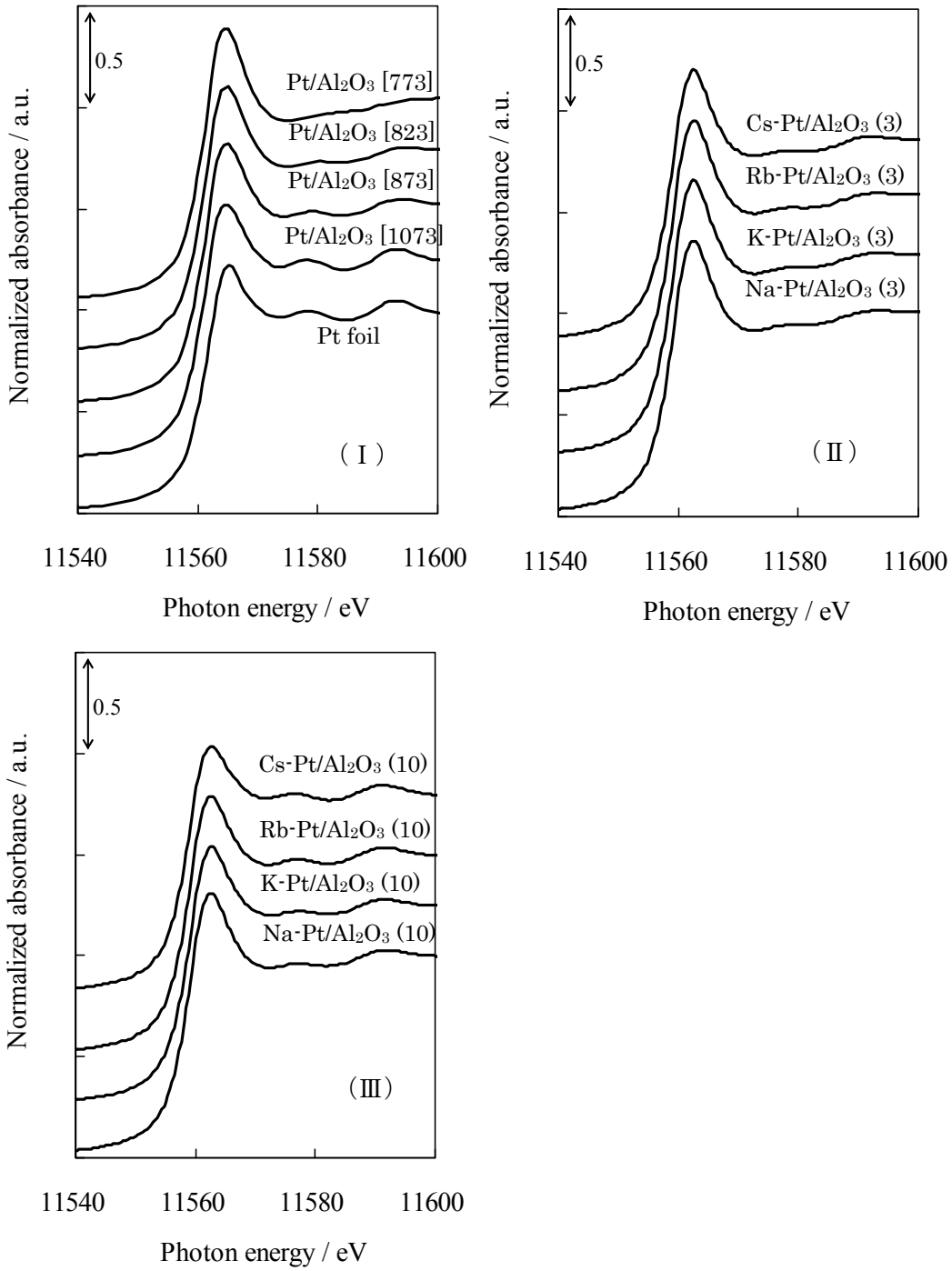

Fig. 3 Pt L_3-edge XANES spectra of the catalysts after H_2 reduction.
(Ⅰ) Pt/Al_2O_3 calcined at various temperatures,
(Ⅱ) M-Pt/Al_2O_3 (3) (M = Na, K, Rb, Cs),
(Ⅲ) M-Pt/Al_2O_3 (10) (M = Na, K, Rb, Cs).

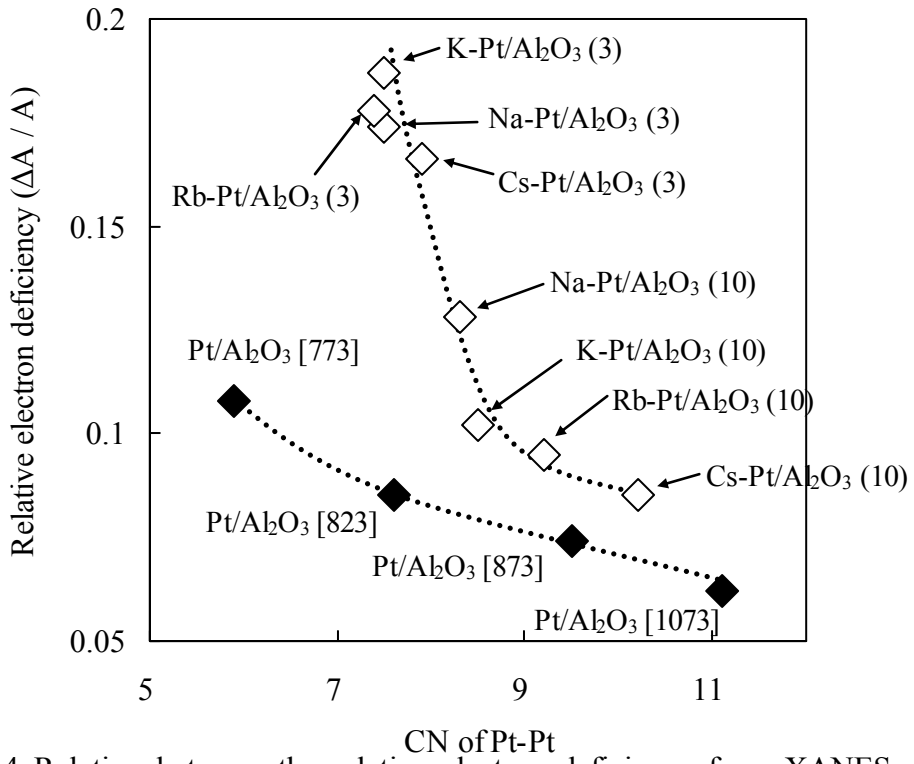

Fig. 4 Relation between the relative electron deficiency from XANES and the coordination number (CN) of the Pt-Pt bond from EXAFS.

(◆) Pt/Al_2O_3 calcined at various temperatures,

(◇) M-Pt/Al_2O_3 (3 and 10) (M = Na, Ka, Rb, Cs).

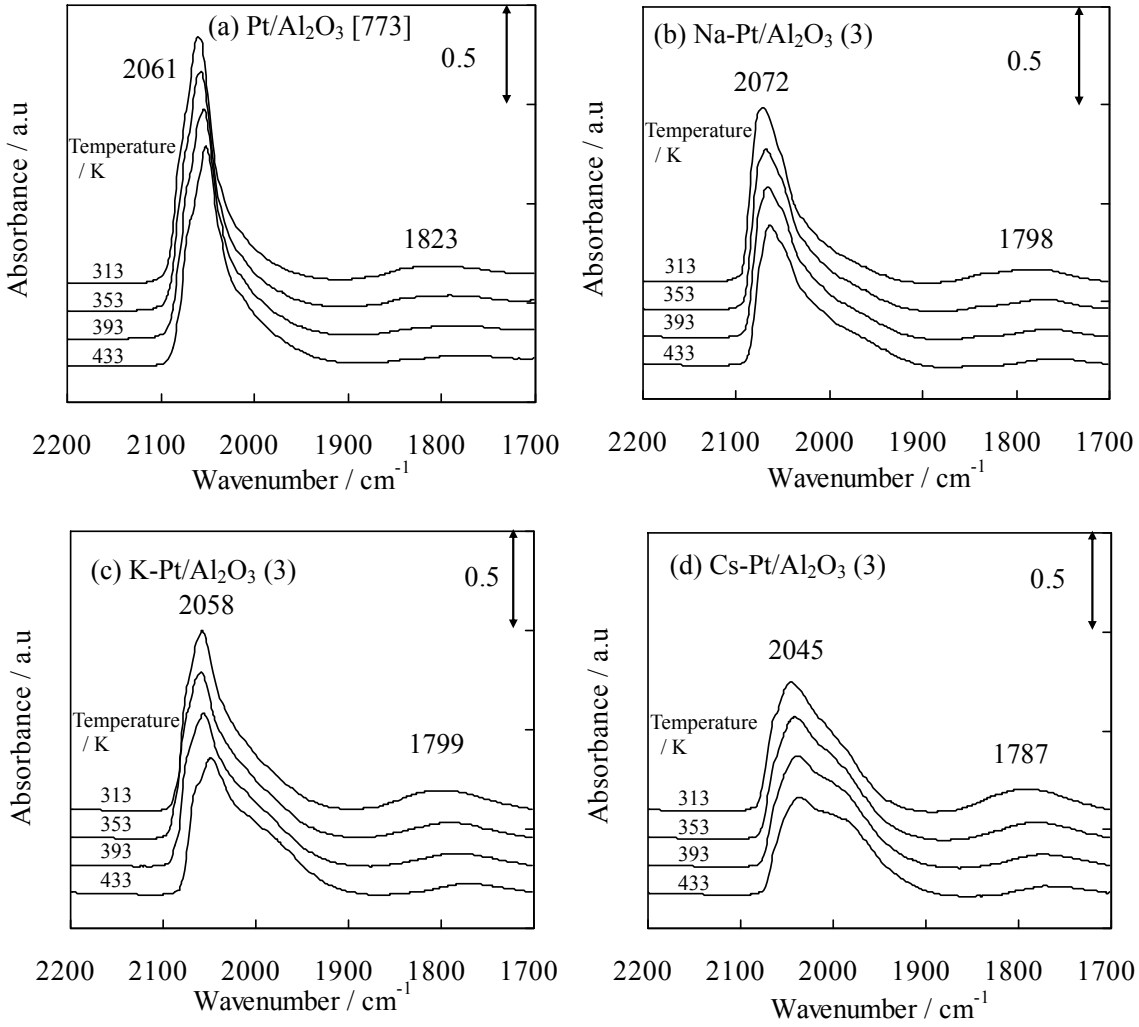

Fig. 5 Effect of evacuation temperature on IR spectra of adsorbed CO on Pt/Al_2O_3 [773] and M-Pt/Al_2O_3 (3) catalysts. The samples were exposed to 0.3 kPa CO at 313 K and evacuated.

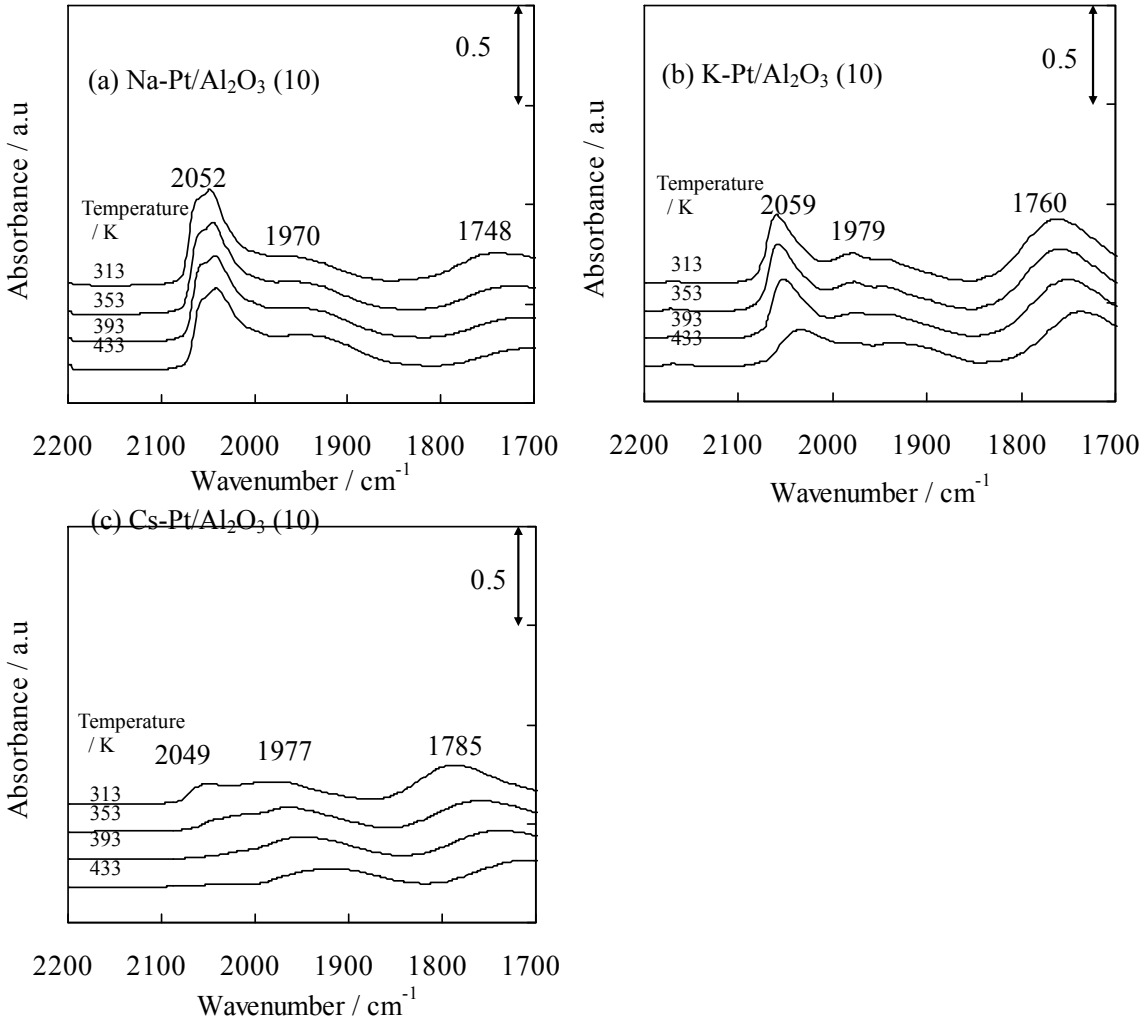

Fig. 6 Effect of evacuation temperature on IR spectra of adsorbed CO on M-Pt/Al_2O_3 (10) catalysts. The samples were exposed to 0.3 kPa CO at 313 K and evacuated.

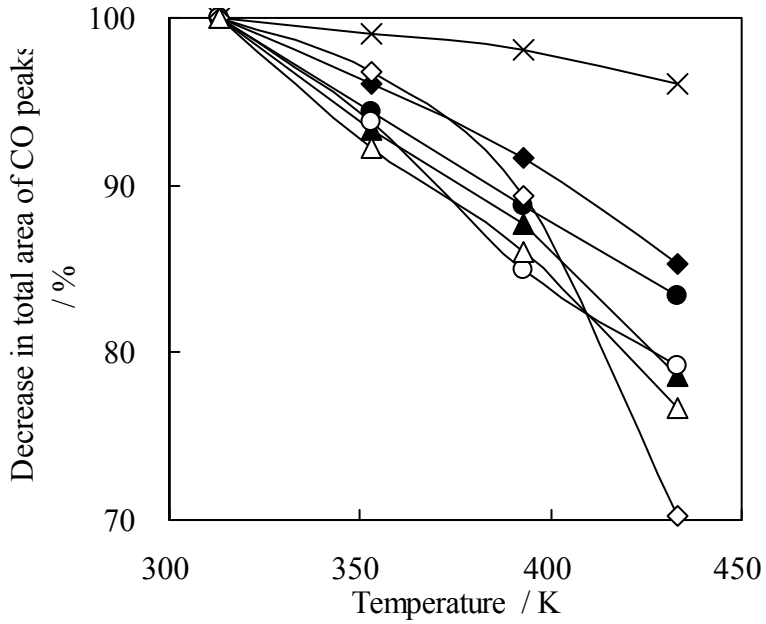

Fig. 7 Effect of evacuation temperature on the decrease in the total area of the CO peaks (Figs. 5 and 6). Pt/Al_2O_3 (×), Na-Pt/Al_2O_3 (3 (●) and 10 (○)), K-Pt/Al_2O_3 (3 (◆) and 10 (◇)), Cs-Pt/Al_2O_3 (3 (▲) and 10 (△)). The samples were exposed to 0.3 kPa CO at 313 K and evacuated.

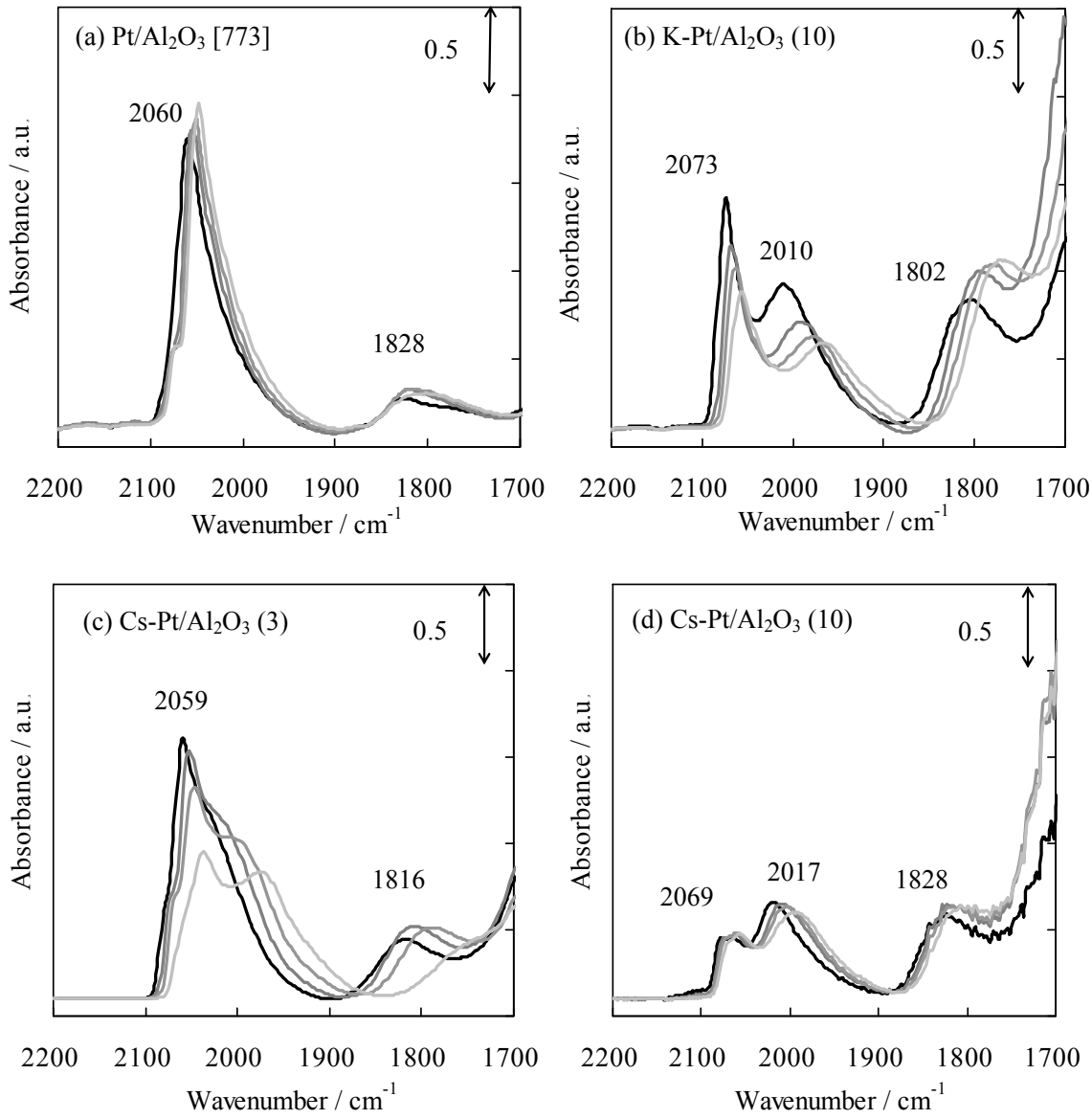

Fig. 8 Effect of reaction temperature on IR spectra of the catalysts under the PROX condition (0.2% CO, 0.2% O_2, 75 % H_2, He balance).

___ : 313 K, ___ : 353 K, ___ : 393 K, ___ : 433 K.